Radio Science, Volume 20, Number 5, Pages 1069–1089, September–October 1985

An updated model for millimeter wave propagation in moist air

Hans J. Liebe

National Telecommunications and Information Administration, Institute for Telecommunication Sciences, Boulder, Colorado

(Received December 11, 1984; revised March 26, 1985; accepted March 26, 1985.)

A practical atmospheric Millimeter-Wave Propagation Model (MPM) is formulated that predicts attenuation, delay, and noise properties of moist air for frequencies up to 1000 GHz. Input variables are height distributions (0–30 km) of pressure, temperature, humidity, and suspended droplet concentration along an anticipated radio path. Spectroscopic data consist of more than 450 parameters describing local O_2 and H_2O absorption lines complemented by continuum spectra for dry air, water vapor, and hydrosols. For a model (MPM*) limited to frequencies below 300 GHz, the number of spectroscopic parameters can be reduced to less than 200. Recent laboratory measurements by us at 138 GHz of absolute attenuation rates for simulated air with water vapor pressures up to saturation allow the formulation of an improved, though empirical water vapor continuum. Model predictions are compared with selected (2.5–430 GHz) data from both laboratory and field experiments. In general, good agreement is obtained.

1. INTRODUCTION

Atmospheric propagation limitations dominate most considerations in the advancement of millimeter wave applications [*Crane*, 1981]. Adverse weather causes millimeter-wave signal degradations due to rain, wet snow, suspended particles, and water vapor. A propagation model provides a cost-effective means of predicting the performance of a system for its intended use by taking into account limiting factors of the atmosphere that in the actual operating environment may be difficult to identify. The object of a model is to encompass the broadest collection of observable phenomena under the least number of postulates. This leads to an array of individual routines, each taking the most practical simulation approach to a particular propagation hindrance. Models of this nature have been reported by *Waters* [1976], *Zrazhevskiy* [1976], *Falcone et al.* [1982] (FASCODE), *Duncan et al.* [1981], and *Duncan and Steinhoff* [1982] (EOSAEL).

The Institute for Telecommunication Sciences (ITS) has developed a Millimeter-wave Propagation Model (MPM) that relates easy-to-obtain meteorological variables to difficult-to-measure propagation factors (attenuation, delay, and medium noise up to 1000 GHz) in most direct manner [*Liebe*, 1983*a*]. The atmospheric medium is described by measurable quantities for which spatial and temporal statistics are assumed to be known. The modular ITS program MPM has found a place in work by *Allen et al.* [1983], *Brussaard et al.* [1983], *Clark et al.* [1984], *Manabe et al.* [1984], *Mizushima* [1982], *Pierluissi et al.* [1982], *E. W. Smith* [1981], *E. K. Smith* [1982], among others.

This paper addresses the moist air portion of the MPM routine. Central to the routine are more than 450 spectroscopic parameters, some of which have been altered to accommodate new research findings. Since these revisions impact the predictions, we present here an update of the earlier version [*Liebe*, 1981] using similar notation. Included in the discussion is a reduced line data base for more computer-efficient MPM predictions below 300 GHz. Modeling results are then compared with data from recent experiments and a theoretical treatment.

Paper number 5S0280.

2. MILLIMETER-WAVE PROPAGATION MODEL (MPM)

Meteorological variables

Gaseous oxygen (O_2), water vapor (H_2O) and suspended water droplets (hydrosols) are considered to be the principal absorbers in moist air. The physical state of air is described by four measurables P-T-RH-w which relate to the internal model variables p-θ-$e(v)$-w_0 as follows:

$$\mathbf{P} = p + e \qquad \mathbf{T} = 300/\theta$$

$$\mathbf{RH} = (e/e_s)100 = (v/v_s)100 \qquad \mathbf{w} = w_0\, G(RH)$$

Barometric pressure is labeled P, p is dry air pressure and e is partial water vapor pressure, all in units of kilopascal (1 kPa = 10 mbar); temperature T in degrees Kelvin (K) is converted to a relative inverse temperature parameter θ; relative humidity

$$\mathrm{RH} = (e/e_s)100 = 41.51(e/\theta^5)10^{(9.834\theta^{-10})} \leq 100\% \tag{1}$$

($\leq 0.1\%$ approximation between $\pm 40°\mathrm{C}$ of saturation pressure e_s over liquid phase) is given as absolute humidity ratio described by partial vapor pressure e; dry air and vapor densities are expressed by

$$u = 11.612p\theta \qquad v = 7.217e\theta \qquad \mathrm{g/m^3} \tag{2}$$

the vapor mixing ratio is v/u; and a dry mass concentration of hygroscopic aerosol is w_0 in grams per cubic meter. An approximate expression for the humidity-dependent growth factor is for RH < 96% given by [*Haenel*, 1976]

$$G \cong 100/(100 - \mathrm{RH}) \tag{3}$$

Complex refractivity N

The heart of the model is a macroscopic measure of interactions between radiation and absorbers expressed as complex refractivity in N units (i.e., ppm $\equiv 10^{-6}$)

$$\mathbf{N} = N_0 + N'(f) + jN''(f) \tag{4}$$

The refractivity consists of a frequency-independent term N_0 plus various spectra of refractive dispersion $N'(f)$ and absorption $N''(f)$. In radio engineering it is customary to express the imaginary part of (4) as specific power attenuation α and the real part as propagation delay β (with reference to vacuum); that is,

$$\alpha = 0.1820 f N''(f) \qquad \mathrm{dB/km} \tag{5a}$$

and

$$\beta = 3.336[N_0 + N'(f)] \qquad \mathrm{ps/km} \tag{5b}$$

where frequency f is in gigahertz (GHz) throughout.

The calculation of N for frequencies up to 1000 GHz consists of several additive parts:

radio refractivity of air,

$$N_0 = (2.588p + 2.39e)\theta + N_v \tag{6}$$

is defined to be $N = N_0$ at $f = 0$, but has been measured accurately at microwave frequencies when the spectra $N(f)$ are either zero (N_2, Ar, CO_2) or negligible (H_2O, O_2) [e.g., *Boudouris*, 1963; *Liebe et al.*, 1977, Table 2]. Contributions from the rotational spectrum of water vapor are measured to be

$$N_v = 41.6e\theta^2 \tag{7}$$

while theory predicts a value for N_v, which is 4.35% lower [*Hill et al.*, 1982]; resonance information for $n_a = 48$ oxygen lines; resonance information for $n_b = 30$ water vapor lines; continuum absorption (N_e) presumed to be from far-wing contributions of many (>100) strong H_2O lines falling in the frequency range 1–30 THz (see section 3.4); continuum due to nonresonant O_2 and pressure-induced N_2 absorption (N_p); suspended water droplets (hydrosols) (N_w).

Absorption and dispersion spectra are obtained from line-by-line calculations plus various continuum spectra N_p (dry air), N_e (water vapor), and N_w (hydrosols) according to

$$N''(f) = \sum_{i=1}^{n_a} (SF'')_i + N''_p + \sum_{i}^{n_b} (SF'')_i + N''_e + N''_w \tag{8a}$$

and

$$N'(f) = \sum_{i=1}^{n_a} (SF')_i + N'_p + \sum_{i}^{n_b} (SF')_i + N'_e + N'_w \tag{8b}$$

where S is the line strength in kilohertz and F' and F'' are real and imaginary parts of a line shape function in GHz^{-1}. Pressure broadening of the dominant lines leads to two different types of frequency responses, namely, sharp resonance lines and continuum spectra. Both are treated in the following for atmospheric conditions up to heights of $h = 30$ km. Self- and foreign-gas-broadening influences have to be taken into account. Trace gas spectra are neglected since their strength is too small to markedly affect propagation, at least below $h \cong 15$ km. A radio path is nominally from ground to space.

2.1. *Local line absorption and dispersion*

The Van Vleck-Weisskopf function was modified by *Rosenkranz* [1975] to describe, to first order, line overlap effects. This leads to local absorption and dispersion line profiles in the form

$$F''(f) = \left(\frac{1}{X} + \frac{1}{Y}\right)\frac{\gamma f}{\nu_0} - \delta\left[\frac{\nu_0 - f}{X} + \frac{\nu_0 + f}{Y}\right]\frac{f}{\nu_0} \tag{9a}$$

and (R. Hill, personal communications, 1984)

$$F'(f) = \frac{Z - f}{X} + \frac{Z + f}{Y} - \frac{2}{\nu_0} + \delta\left[\frac{1}{X} - \frac{1}{Y}\right]\frac{\gamma f}{\nu_0} \tag{9b}$$

with the abbreviations

$$X = (\nu_0 - f)^2 + \gamma^2 \qquad Y = (\nu_0 + f)^2 + \gamma^2$$

$$Z = (\nu_0^2 + \gamma^2)/\nu_0$$

The line parameters are calculated according to the scheme below:

Symbol	O_2 Lines in Air	H_2O Lines in Air	
S, kHz	$a_1 p\theta^3 \exp[a_2(1-\theta)]$	$b_1 e\theta^{3.5} \exp[b_2(1-\theta)]$	(10)
γ, GHz	$a_3(p\theta^{(0.8-a_4)} + 1.1e\theta)$	$b_3(p\theta^{0.8} + 4.80e\theta)$	(11)
δ	$a_5 p\theta^{a_6}$	0	(12)

Line center frequencies ν_0 and the spectroscopic coefficients $a_1(\geq 10^{-7}$ Hz/Pa) to a_6, and $b_1(\geq 10^{-3}$ Hz/Pa) to b_3 for strength S, width γ, and overlap correction δ are listed in Table 1. A discussion of the revisions to a and b coefficients with respect to the 1981 MPM version follows in section 2.4.

Standard line shapes $F''(f)$, including the modified Van Vleck-Weisskopf function (9), predict in frequency regions of local line dominance about the same results for $N''(f)$ as long as $F''(f)$ exceeds by 0.1% the peak value at $f = \nu_0$. Far-wing contributions of smaller magnitude depend very much upon the chosen shape function [*Liebe*, 1984]. So far, no line shape has been confirmed that predicts absorption intensities over ranges 10^{-3} to $<10^{-6}$ of $F''(\nu_0)$, as required for the water vapor spectrum. Expected far-wing contributions from strong infrared lines, where $\alpha(\nu_0) > 10^5$ dB/km, are accounted for summarily by empirical correction.

2.2. *Continuum spectra for air*

Continuum spectra in (8) identify dry air and water vapor terms $N_p + N_e$ and must be added to the selected group of local O_2 and H_2O resonance lines (Table 1) described by (9) in order to correctly predict atmospheric millimeter wave attenuation in window ranges between lines. Continuum absorption increases monotonically with frequency.

The dry air continuum

$$N_p''(f) = (2a_0\{\gamma_0[1 + (f/\gamma_0)^2][1 + (f/60)^2]\}^{-1} + a_p p\theta^{2.5})fp\theta^2 \tag{13a}$$

and

$$N_p'(f) = a_0\{[1 + (f/\gamma_0)^2]^{-1} - 1\}p\theta^2 \tag{13b}$$

make a small contribution at ground level pressures due to the nonresonant O_2 spectrum below 10 GHz [*Mingelgrin*, 1974] and a pressure-induced N_2 spectrum, effective above 100 GHz [*Stankevich*, 1974]. A width parameter for the Debye spectrum of O_2 is formulated in accordance with (11) to be $\gamma_0 = 5.6 \times 10^{-3}(p + 1.1e)\theta^{0.8}$(GHz) [*Rosenkranz*, 1982]. The continuum coefficients are $a_0 = 3.07 \times 10^{-4}$ [*Rosenkranz*, 1975] and $a_p \cong 1.40(1\text{–}1.2f^{1.5}10^{-5})10^{-10}$ [*Stone et al.*, 1984].

The water vapor continuum is derived empirically from fitting experimental data in the case of N_e'' and based on theoretical data in the case of N_e', leading to

$$N_e''(f) = [b_f p + b_e e\theta^3]fe\theta^{2.5} \tag{14a}$$

and

$$N_e'(f) \cong b_0 f^{2.05} e\theta^{2.4} \tag{14b}$$

where $b_f = 1.40 \times 10^{-6}$, $b_e = 5.41 \times 10^{-5}$, and $b_0 = 6.47 \times 10^{-6}$.

Water vapor continuum absorption has been a major source of uncertainty in predicting millimeter wave attenuation rates, especially in the window ranges [*Bohlander et al.*, 1985]. Recent laboratory experiments employing a special high-humidity spectrometer at $f = 138$ GHz, RH = 80–100%, and $p_1 =$ 0–150 kPa (nitrogen) led to the following results [*Liebe*, 1984]: equation (14*a*) is needed to supplement local line (Table 1) contributions; the coefficient b_f is valid only for the selected local line base treated with line shape (9); the strong self-broadening component $b_e e^2$ is nearly unaffected by (9) (see section 3.4); coefficient b_f was adjusted ($\times 0.915$) for air broadening. The coefficient b_0 and both exponents in (14*b*) were obtained by fitting dispersion results of line-by-line calculations for the rotational H_2O spectrum above 1 THz (R. Hill, personal communication, 1984).

2.3. *Hydrosol continuum (haze and fog)*

Suspended water droplets (hydrosols) in haze and fog (or clouds) are millimeter wave absorbers. Their size range of radii is below 50 μm, which allows the Rayleigh approximation of Mie scattering theory to be used for calculating refractivity contributions N_w to (8) in the form [*Liebe*, 1981; *Falcone et al.*, 1982]

$$N_w''(f) = 4.50w/\varepsilon''(1 + \eta^2) \tag{15a}$$

and

$$N_w'(f) \cong 2.4 \times 10^{-3}\, w\varepsilon' \tag{15b}$$

where $\eta = (2 + \varepsilon')/\varepsilon''$; and ε', ε'' are real and imaginary parts of the dielectric constant for water. For

TABLE 1. Oxygen and Water Vapor Line Parameters for a Local Line Base LB in Air Below 1000 GHz, and Selected Lines (*) for a Reduced-Base LB* to be Used Below 300 GHz

ν_0, GHz	a_1, kHz/kPa	a_2	a_3, GHz/kPa	a_4	a_5, 1/kPa	a_6	LB*
49.452379	0.12 E-6	11.830	8.40 E-3	0	5.60 E-3	1.7	
49.962257	0.34 E-6	10.720	8.50 E-3	0	5.60 E-3	1.7	
50.474238	0.94 E-6	9.690	8.60 E-3	0	5.60 E-3	1.7	
50.987748	2.46 E-6	8.690	8.70 E-3	0	5.50 E-3	1.7	
51.503350	6.08 E-6	7.740	8.90 E-3	0	5.60 E-3	1.8	*
52.021409	14.14 E-6	6.840	9.20 E-3	0	5.50 E-3	1.8	*
52.542393	31.02 E-6	6.000	9.40 E-3	0	5.70 E-3	1.8	*
53.066906	64.10 E-6	5.220	9.70 E-3	0	5.30 E-3	1.9	*
53.595748	124.70 E-6	4.480	10.00 E-3	0	5.40 E-3	1.8	*
54.129999	228.00 E-6	3.810	10.20 E-3	0	4.80 E-3	2.0	*
54.671157	391.80 E-6	3.190	10.50 E-3	0	4.80 E-3	1.9	*
55.221365	631.60 E-6	2.620	10.79 E-3	0	4.17 E-3	2.1	*
55.783800	953.50 E-6	2.115	11.10 E-3	0	3.75 E-3	2.1	*
56.264777	548.90 E-6	0.010	16.46 E-3	0	7.74 E-3	0.9	*
56.363387	1344.00 E-6	1.655	11.44 E-3	0	2.97 E-3	2.3	*
56.968180	1763.00 E-6	1.255	11.81 E-3	0	2.12 E-3	2.5	*
57.612481	2141.00 E-6	0.910	12.21 E-3	0	0.94 E-3	3.7	*
58.323874	2386.00 E-6	0.621	12.66 E-3	0	−0.55 E-3	−3.1	*
58.446589	1457.00 E-6	0.079	14.49 E-3	0	5.97 E-3	0.8	*
59.164204	2404.00 E-6	0.386	13.19 E-3	0	−2.44 E-3	0.1	*
59.590982	2112.00 E-6	0.207	13.60 E-3	0	3.44 E-3	0.5	*
60.306057	2124.00 E-6	0.207	13.82 E-3	0	−4.13 E-3	0.7	*
60.434775	2461.00 E-6	0.386	12.97 E-3	0	1.32 E-3	−1.0	*
61.150558	2504.00 E-6	0.621	12.48 E-3	0	−0.36 E-3	5.8	*
61.800152	2298.00 E-6	0.910	12.07 E-3	0	−1.59 E-3	2.9	*
62.411212	1933.00 E-6	1.255	11.71 E-3	0	−2.66 E-3	2.3	*
62.486253	1517.00 E-6	0.078	14.68 E-3	0	−4.77 E-3	0.9	*
62.997974	1503.00 E-6	1.660	11.39 E-3	0	−3.34 E-3	2.2	*
63.568515	1087.00 E-6	2.110	11.08 E-3	0	−4.17 E-3	2.0	*
64.127764	733.50 E-6	2.620	10.78 E-3	0	−4.48 E-3	2.0	*
64.678900	463.50 E-6	3.190	10.50 E-3	0	−5.10 E-3	1.8	*
65.224067	274.80 E-6	3.810	10.20 E-3	0	−5.10 E-3	1.9	*
65.764769	153.00 E-6	4.480	10.00 E-3	0	−5.70 E-3	1.8	*
66.302088	80.09 E-6	5.220	9.70 E-3	0	−5.50 E-3	1.8	*
66.836827	39.46 E-6	6.000	9.40 E-3	0	−5.90 E-3	1.7	*
67.369595	18.32 E-6	6.840	9.20 E-3	0	−5.60 E-3	1.8	*
67.900862	8.01 E-6	7.740	8.90 E-3	0	−5.80 E-3	1.7	*
68.431001	3.30 E-6	8.690	8.70 E-3	0	−5.70 E-3	1.7	
68.960306	1.28 E-6	9.690	8.60 E-3	0	−5.60 E-3	1.7	
69.489021	0.47 E-6	10.720	8.50 E-3	0	−5.60 E-3	1.7	
70.017342	0.16 E-6	11.830	8.40 E-3	0	−5.60 E-3	1.7	
118.750341	945.00 E-6	0.000	15.92 E-3	0	−0.44 E-3	0.9	*
368.498350	67.90 E-6	0.020	19.20 E-3	0.6	0	1	
424.763120	638.00 E-6	0.011	19.16 E-3	0.6	0	1	
487.249370	235.00 E-6	0.011	19.20 E-3	0.6	0	1	
715.393150	99.60 E-6	0.089	18.10 E-3	0.6	0	1	
773.838730	671.00 E-6	0.079	18.10 E-3	0.6	0	1	
834.145330	180.00 E-6	0.079	18.10 E-3	0.6	0	1	

TABLE 1. (continued)

ν_0, GHz	b_1, kHz/kPa	b_2	b_3, GHz/kPa	LB*
22.235080	0.1090	2.143	27.84 E-3	*
67.813960	0.0011	8.730	27.60 E-3	
119.995940	0.0007	8.347	27.00 E-3	
183.310117	2.3000	0.653	28.35 E-3	*
321.225644	0.0464	6.156	21.40 E-3	
325.152919	1.5400	1.515	27.00 E-3	*
336.187000	0.0010	9.802	26.50 E-3	
380.197372	11.9000	1.018	27.60 E-3	
390.134508	0.0044	7.318	19.00 E-3	
437.346667	0.0637	5.015	13.70 E-3	
439.150812	0.9210	3.561	16.40 E-3	
443.018295	0.1940	5.015	14.40 E-3	
448.001075	10.6000	1.370	23.80 E-3	
470.888947	0.3300	3.561	18.20 E-3	
474.689127	1.2800	2.342	19.80 E-3	
488.491133	0.2530	2.814	24.90 E-3	
503.568532	0.0374	6.693	11.50 E-3	
504.482692	0.0125	6.693	11.90 E-3	
556.936002	510.0000	0.114	30.00 E-3	
620.700807	5.0900	2.150	22.30 E-3	
658.006500	0.2740	7.767	30.00 E-3	
752.033227	250.0000	0.336	28.60 E-3	
841.073593	0.0130	8.113	14.10 E-3	
859.865000	0.1330	7.989	28.60 E-3	
899.407000	0.0550	7.845	28.60 E-3	
902.555000	0.0380	8.360	26.40 E-3	
906.205524	0.1830	5.039	23.40 E-3	
916.171582	8.5600	1.369	25.30 E-3	
970.315022	9.1600	1.842	24.00 E-3	
987.926764	138.0000	0.178	28.60 E-3	

frequencies above 300 GHz, the following approximation

$$N''_w(f) \cong 0.55wf^{-0.1}\theta^{-6} \tag{15c}$$

can be used instead of (15*a*), based on data reported by *Simpson et al.* [1979].

The dielectric constant of water is calculated with the Debye model reported by *Chang and Wilheit* [1979], which is valid for $f \leq 300$ GHz:

$$\varepsilon'' = (185 - 113/\theta)f\tau/[1 + (f\tau)^2] \tag{16a}$$

and

$$\varepsilon' = 4.9 + (185 - 113/\theta)/[1 + (f\tau)^2] \tag{16b}$$

where $\tau = 4.17 \times 10^{-5}\theta \exp(7.13\,\theta)$ ns.

Haze conditions are related to vapor-to-droplet conversion processes reversible (swelling/shrinking) with relative humidity for values below RH = 100%. The simple growth function (3) provides an approximation of the conversion up to RH $\cong$ 96% and typical dry air mass loadings of hygroscopic aerosol in ground level air are below $w_0 \cong 10^{-4}$ g/m^3. A practical growth function covering the range RH = 96 to >100% is lacking. Such function is needed to model the growth of hydrosols to values $w = 10^{-3}$ to 1 g/m^3 as observed under various fog conditions. At present, values for w are assumed in (15) and the contributions added to calculations (8) for saturated (100% RH) air.

2.4. *Discussion of spectroscopic parameters*

Recent relevant references were scrutinized for the purpose of updating the spectroscopic data base of

TABLE 2. Measured Width γ^0 and Broadening Efficiency m at 300 K for 10 Selected Millimeter-Wave Lines of O_2 Using 19 Different Broadener Molecules X

	Frequency f, GHz										
Molecule X	425	119	58.5	59.6	59.2	61.2	61.8	57.0	63.0	55.8	61.0
Quantum ID	$2_1 \rightarrow 2_3$	1−	3+	5+	7−	9+	11+	13−	15+	17−	
$O_2 - O_2$ width γ^0,	11.9(12)*	15.8	14.8	14.0	13.7	13.1	12.7	12.5	12.2	12.0	2.385§
MHz/kPa	19.6(20)†	22.9†	···	···	···	···	···	···	···	···	
					Broadening Efficiency $m(O_2 - X)$						
Air	···	···	0.99	0.98	0.98	0.97	0.98	0.96	0.95	···	2.588 (equation (6))
	1.61(18)‡	1.01(5)‡	0.983‡	0.975‡	0.952‡	0.966‡	0.959‡	0.935‡	0.927‡	0.94‡	
	1.05(10)†	0.94†	···	···	···	···	···	···	···	···	
Noble											
He	···	0.753	0.72	0.73	0.74	0.73	0.75	0.75	0.77	···	0.317
Ne	···	···	0.62	0.63	0.62	0.63	0.62	0.60	0.58	···	0.608
Ar	···	0.945	0.85	0.83	0.82	0.77	0.78	0.77	0.72	0.69	2.493
Kr	···	···	0.84	0.83	0.81	0.81	0.78	0.74	0.70	···	3.81
Xe	···	···	0.92	0.90	0.89	0.89	0.83	0.77	0.72	···	6.068
Diatomic											
D_2	···	···	1.01	···	···	···	···	···	1.02	···	1.21
H_2	···	···	1.13	1.10	1.12	1.15	1.19	···	1.18	···	1.22
N_2	1.78(20)	1.03(5)	0.98	0.97	0.94	0.96	0.95	0.95	0.92	0.93	2.640 (reference)
	1.06(10)†	0.928†	···	···	···	···	···	···	···	···	
NO	···	···	1.00	···	···	···	···	···	0.98	···	3.00
CO	···	···	1.00	···	···	···	···	···	0.93	···	3.17
Triatomic											
CO_2	···	···	1.15	1.12	···	···	···	···	1.09	···	4.450
N_2O	···	···	1.16	···	···	···	···	···	1.11	···	5.02
H_2O	···	1.08(12)	···	···	···	1.2(1)	···	···	···	···	44.0 (equation (7))
Alkane											
CH_4	···	···	1.17	1.21	1.19	1.19	1.18	···	1.14	···	3.98
C_2H_2	···	···	1.29	···	···	···	···	···	1.12	···	6.67
C_2H_6	···	···	1.35	···	···	···	···	···	1.29	···	6.63
C_3H_8	···	···	1.41	···	···	···	···	···	1.33	···	9.241
C_4H_{10}	···	···	1.53	···	···	···	···	···	1.46	···	11.96

H. Liebe and G. Gimmestad (personal communication, 1977); *Setzer and Pickett* [1977]; *Pickett et al.* [1981]. In addition, the associated refractivities N_0/p are given as measured at 61 GHz for the pure gas. Experimental conditions: $p(O_2) = 0.5$ and $p(X) = 0$–1.2 kPa, $f = \nu_0 \pm 5$ MHz, $H \simeq 0$ G.

§Refractivity N_0/p, ppm/kPa.

*Digits in parentheses give the standard deviation from the mean in terms of the final listed digits; uncertainty of all other data is less than 3%.

†*Pickett et al.* [1981], 207 K.

‡$m \sum_{i=1}^{4} (mr)_i$ with the air abundances: $r_1(N_2) = 0.78084$, $r_2(O_2) = 0.209476$, $r_3(Ar) = 0.00934$, $r_4(CO_2) = 0.000322$.

the 1981 MPM routine. Improvements have been made to $\nu_0(O_2)$ [*Endo and Mizushima*, 1982), a_1 [*Liebe*, 1983*a*], $a_3(e)$ [*Setzer and Pickett*, 1977], a_4 [*Pickett et al.*, 1981]; and $\nu_0(H_2O)$ [*Messer et al.*, 1983, 1984; *Steenbeckeliers and Bellet*, 1971]; $b_3(\theta)$ [*Thomas and Nordstrom*, 1982].

The dry air coefficients a_1 to a_5 are based largely on solid experimental evidence obtained at frequencies within 60 GHz band and 119 GHz line cores where α exceeded 0.2 dB/km [*Liebe et al.*, 1977]. Results of additional width (a_3) studies on oxygen lines are summarized in Table 2 for a wide variety of individual broadeners including air. The self-broadened ($O_2 - O_2$) width is γ° in MHz/kPa; the width of binary gas mixtures ($O_2 - X$) is $m\gamma^\circ$, where m is the broadening efficiency of the foreign gas X [*Smith and Guiraud*, 1979, 1981]. The overlap coefficients a_5 evolve from an iterative procedure [*Rosenkranz*, 1975]. Temperature dependence was evaluated over the range $T = 200$ to 300 K and the results were approximated by a_6 (12). A more rigorous theory for overlap corrections δ has been devel-

oped by *Smith* [1981] which to first order reduces to Rosenkranz's approach adapted here.

The MPM version for local (<1000 GHz) atmospheric water vapor lines requires 120 spectroscopic coefficients since overlap corrections need not be made [*Lam*, 1977]. All water vapor coefficients b_1, b_2, and $b_3(T_0 = 300\ \text{K})$ are derived from the Air Force Geophysical Laboratory (AFGL) tape ($T_0 = 296$ K) [*Rothman et al.*, 1983]. Conversion from molecular (S_M, E_l, Γ) to radio engineering ($b_{1,2,3}$) units is accomplished via

$$\begin{aligned} b_1 &= 5.385(S_M/\nu_0)10^{24} \exp(0.0133 b_2) \quad \text{kHz/kPa} \\ b_2 &= 4.796 \times 10^{-3} E_l \\ b_3 &= 0.2927\Gamma \quad \text{GHz/kPa} \end{aligned} \tag{17}$$

where ν_0 is in GHz, S_M in cm^{-1} $(\text{molec/cm}^2)^{-1}$, E_l in cm^{-1}, and Γ in cm^{-1}/atm. Uncertainties in the theoretical line strength value S_M have been estimated to be about 15% [*Rothman et al.*, 1983]. Comparisons with other reported H_2O line data bases [*Flaud et al.*, 1981; *Poynter and Pickett*, 1981; *Mizushima*, 1982] lie within this limit. Line width data b_3 for the 22 GHz and 183 GHz lines are based on laboratory experiments [see *Liebe and Dillon*, 1969]. Theory predicts the possibility of pressure-induced shifts ξ of the line center frequency to $(\nu_0 + \xi)$. For the self-broadened 22.3 and 752 GHz H_2O lines, "blue" shifts of the order of $\xi = (2\text{–}4)b_3 e \times 10^{-4}$ (GHz) have been reported [*Liebe and Dillon*, 1969; *Belov et al.*, 1983]. This small shift effect is neglected.

2.5. *Radio path behavior*

The program MPM was developed for ground-to-ground and ground-to-space applications in telecommunications, radio astronomy, remote sensing, etc., within the 1–1000 GHz range. Wave propagation over a radio path can be described by three principal quantities when increments dx of the total path length L, both in kilometers, are assumed in the x direction:

cumulative path attenuation A

$$A = \int_0^L \alpha(x)\, dx \quad \text{dB} \tag{18a}$$

or transmission factor $\mathbf{T}$

$$\mathbf{T} = \exp(-0.2303A) \tag{18b}$$

cumulative path delay B

$$B = \int_0^L \beta(x)\, dx \quad \text{ps} \tag{19a}$$

refractive path delay B_0

$$B_0 = 3.336 \int_0^L N_0(x)\, dx \quad \text{ps} \tag{19b}$$

and sky noise T_B

$$T_B = \int_{h_0}^{\infty} T(x) WF(x)\, dx + 2.7\mathbf{T}(h_0, \infty) \quad \text{K} \tag{20}$$

expressed as equivalent blackbody temperature of radiation by the Rayleigh-Jeans approximation to Planck's law [*Waters*, 1976; *Smith*, 1982]; where

$$WF(x) = 0.2303\alpha(x)\mathbf{T}(x', x) \quad \text{km}^{-1}$$

is a weighting function on $T(x)$, the local ambient temperature along the path; and x' and x are two adjacent points.

Attenuation A quantifies the amount of energy extracted from a plane wave propagating through the atmosphere, delay B is a measure of the excess travelling time with reference to vacuum, and brightness T_B indicates noise emission (between 2.7 K from outer space for $\mathbf{T} = 1$ away from the sun and $T(h_0)$ ambient for $\mathbf{T} = 0$) downwelling the ray path x to the starting level h_0.

The path-integrated densities of water vapor and suspended droplet water, that is,

$$\begin{aligned} V &= 0.1 \int_0^L v(x)\, dx \quad \text{cm} \\ W &= 0.1 \int w(x)\, dx \quad \text{cm} \end{aligned} \tag{21}$$

(1 cm ≡ 1 g/cm^2) are meaningful quantities to correlate with A, B, and T_B. For example, global vapor monthly averages vary between $V \cong 0.5$ (polar regions) and 5.5 cm (equatorial regions) [*Chang et al.*, 1984], and the droplet content of clouds is less than 0.05 V.

The propagation effects (18) to (20) are the desired MPM output; however, these functions cannot be integrated analytically for realistic atmospheric models of $N(x)$, the determining function for α, β, and N_0. Simplifications are introduced that allow the application of numerical methods to three types of radio paths:

Path	Height Range h	$dx =$
horizontal	h_0	L
vertical	h_0 to h_f	Δh
slant	h_0 to h_f	$(\Delta h)s$

The inhomogeneous atmosphere is assumed to be spherically stratified in concentric layers of height intervals Δh, for which values of N can be specified. The atmosphere is structured in discrete height levels (e.g., 48 layers between $h = 0$ and 30 km). Local $P(h)$, $T(h)$, RH(h), and $w(h)$ data are used to calculate for each quasi-homogeneous layer specific values of α, β, and N_0. The MPM can draw P-T-RH-w height profiles from a catalog of 10 model atmospheres and from various fog/cloud models. A numerical integration through the layered medium implies simply a summation of all contributions applying Simpson's rule. A final height level h_f for a path to outer space is defined by atmospheric conditions where $N(h_f) \cong 0$. Selecting $h_f = 30$ km assures that for a zenith path the refractive delay B_0 accounts for better than 99% of the total. Still, there are spectral line contributions to be expected from the range $h = 30$–120 km. They stem foremost from O_2 lines, and are limited to narrow bands (± 50 MHz) around their center frequencies ν_0. The O_2 line shape covering this height range is complicated by Zeeman and Doppler effects [*Liebe*, 1981, 1983*a*].

"Ray tracing" is used for slant paths to determine the path extension factor s. A ray is assumed to start from the initial level h_0 with an elevation angle ψ_0 (measured from the horizontal) and proceeds through the atmosphere gaining the height interval $\Delta h = h - h_0$, while being subjected to refractive bending when $\psi_0 < 90°$. During stable climatic conditions (i.e., a homogeneously stratified atmosphere), the air mass of a slant path down to about $\psi_0 \gtrsim 6°$ increases according to the secant law,

$$s = (\sin \psi_0)^{-1} \tag{22}$$

Zenith ($\psi_0 = 90°$) path behavior is said to be caused by "one" air mass. The effects of both refraction and earth's curvature determine for low-angle ($\psi_0 < 6°$) cases the path increments $(\Delta h)s$, which are calculated from [*Blake*, 1968]

$$s = \left\{1 - \left[\left(\frac{10^6 + N_i}{10^6 + N_j}\right)\left(\frac{r_E + h_0}{r_E + h}\right)\cos \psi_0\right]^2\right\}^{-1/2} \tag{23}$$

where $N_i = [N_0 + N'(f)]_{h_0}$, $N_j = [N_0 + N'(f)]_h$, and $r_E = 6357$ km is a standard (45°N) earth radius. Equation (23) is the spherical form of Snell's law and is strictly valid only when N is purely real. In the case at hand, values for N'' are generally small compared with $N_{i,j} \cong N_0$. For very low elevation angles ($\psi_0 < 1°$) and values of h close to h_0, many fine steps of Δh are required and equation (23) becomes numerically unstable. Approximations of the two terms containing $N_{i,j}$ and r_E are made [e.g., *Blake*, 1968]. At this point, increments $dx = (\Delta h)s$ become very sensitive to the height distributions of meteorological variables. For example, the tangential ($\psi_0 = 0°$) air mass through the U.S. Standard Atmosphere (1976) for dry air is 38 times the zenith value, while for water vapor the tangential mass can vary between 70 and 180 times the zenith value [*Gallery et al.*, 1983].

3. MPM PREDICTIONS

Clear air transmission (18), (19) and emission (20) effects represent ultimate performance limitations to millimeter wave applications. A strong and nonlinear influence of atmospheric humidity RH(T), v(RH), and w(RH) on millimeter-wave attenuation is predicted and will be elucidated by examples. The MPM program was developed for computer-efficient operation by employing only a limited local line data base (Table 1) of the major absorbers H_2O and O_2, supplemented by continuum spectra (13)–(15), and operated from a catalog of P-T-RH-w height profiles or, when available, from in situ data. The wide range of predictions covered by the MPM routine is demonstrated in Figure 1 with examples of air-broadened ($P = 101.3$ kPa) and self-broadened ($p = 0$) attenuation and delay spectra. Four topics are addressed in this section to test the updated MPM program: comparison between attenuation predictions based on (14*a*) and the widely used empirical GR water vapor continuum by Gaut-Reifenstein [*Waters*, 1976; *Liebe*, 1981]; improved computer efficiency for frequencies up to 300 GHz by reducing most H_2O line parameters to a correction term; MPM predictions versus experimental data; comparison with complete line-by-line calculations entailing 17,000 H_2O lines below 150 THz [*Clough et al.*, 1981].

3.1. *The role of water vapor continuum absorption*

Typical sea level behavior of the rates α and β up to 350 GHz is illustrated in Figure 2 for two temperatures (5° and 25°C) and various relative humidities

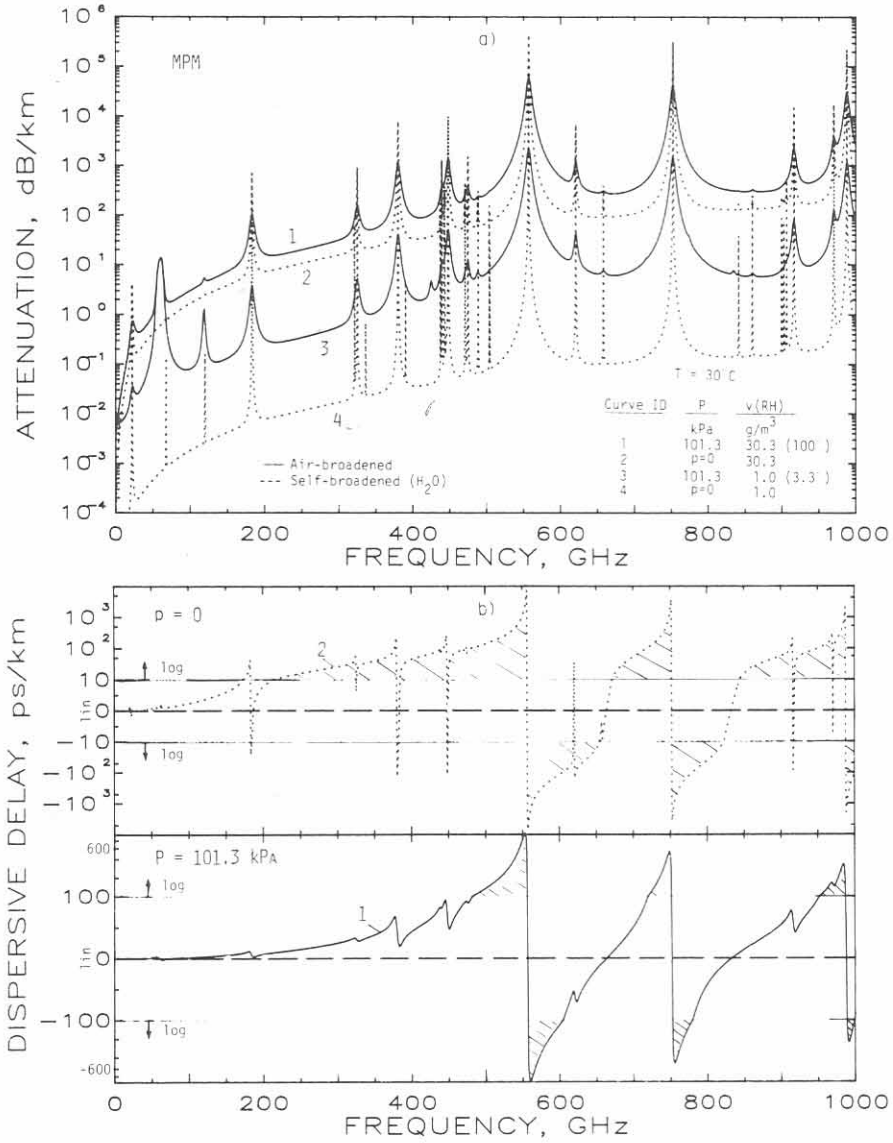

Fig. 1. Predicted (MPM) (*a*) specific attenuation α and (*b*) dispersive delay β up to 1000 GHz for moist sea level air (1 and 3) and pure water vapor (2 and 4) each for two conditions $v = 1$ and 30.3 (100% RH) g/m^3 at $T = 30$°C. (Note the linear-log scales used to display β).

(0–100% RH). Across the millimeter wave spectrum one recognizes more or less transparent window ranges (W1 to W5) separated by molecular resonance peaks. The combined influence of both absolute (v) and relative (RH) humidity upon attenuation rates is made clear by analyzing the temperature dependence of the water vapor attenuation slope $g = [\alpha(v) - \alpha(v = 0)]/v$. Results of $g(T)$ are presented in Figure 3 for two water vapor line peaks and for centers of atmospheric windows W1 to W4 (see Figure 2). Differences at window frequencies between previous modeling attempts using the linear ($\sim vp$) GR continuum and MPM predictions are shown. The strong temperature dependence of g(RH) is caused by the square vapor term in (14*a*), which is accelerated by the temperature-dependent ($\sim T^{18}$!) saturation limit (1).

Corresponding numerical values of specific attenuation α(RH) in Table 3 range for sea level conditions between 0.01 and 150 dB/km. Attenuation α_w due to suspended droplets (Figure 2, curve 9) is added to saturated air conditions that attenuate at rates α_s(100% RH). The selected droplet concentration of $w = 0.1$ g/m^3 is representative of a fog with about 0.3

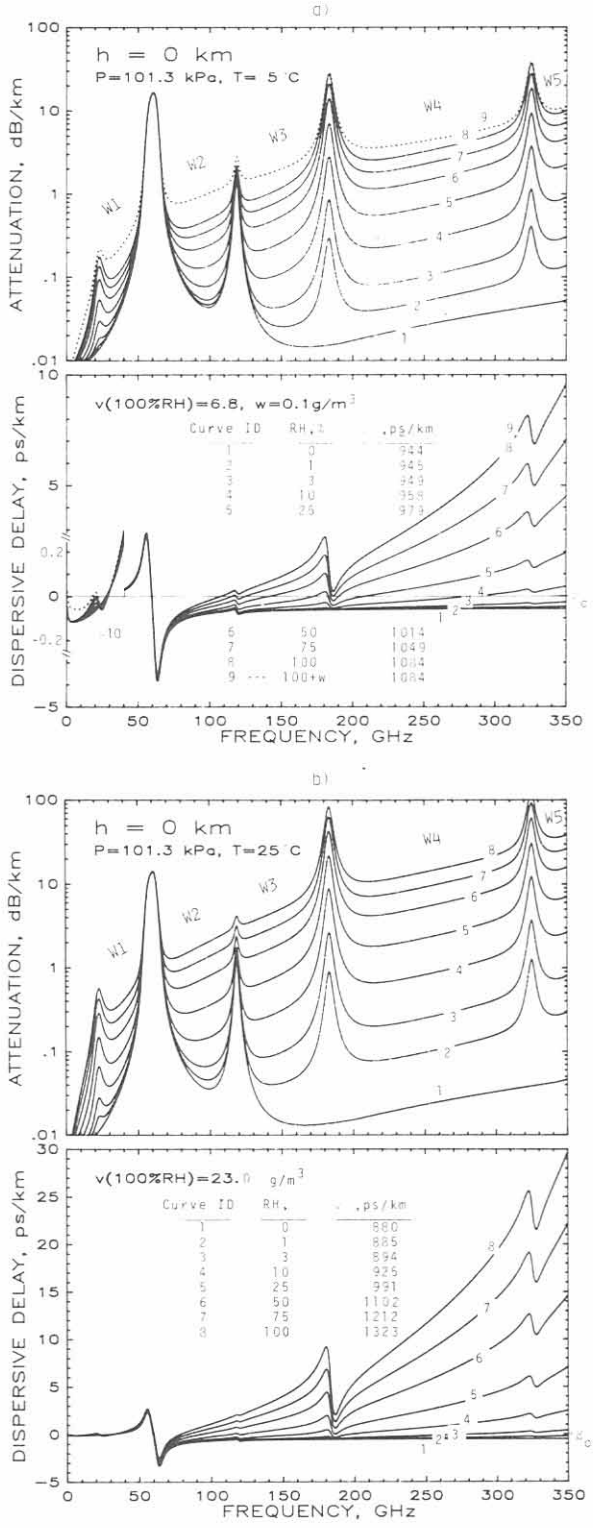

Fig. 2. Predicted specific attenuation α and dispersive delay β ($\beta_0 = 3.336N_0$, refractive delay) for air (0–100% RH) at sea level including a simulated fog conditions ($w = 0.1$) with ~ 300 m visibility. Atmospheric millimeter wave window ranges are marked W1 to W5: (*a*) $T = 5°C$ and $w = 0.1$; (*b*) $T = 25°C$ and $w = 0$.

km optical visibility. A hydrosol factor

$$x_w = (\alpha_w/\alpha_s)(v_s/w) \tag{24}$$

is introduced in Table 3 to demonstrate, particularly in the window ranges, a strong increase in attenuation per unit of H_2O absorbers when vapor molecules convert into droplets. Typically, $w < 0.01$ for haze and $w > 0.01$–1 for fog conditions.

Zenith attenuations A_z(18) and delays B_z (19) at selected frequencies are listed in Table 4 for a model atmosphere (30°N, July) that supports unusually high values of integrated water vapor, $V \leq 7$ cm (21). Differences between MPM and GR-based predictions are, in this case, at the most +27%. Effective heights h_E express zenith attenuation A_z in terms of equivalent horizontal path lengths at h_0.

3.2. *Reduced local line data base*

Transfer properties of moist air set a natural frequency barrier at about 350 GHz to the advancement of a majority of terrestrial system applications. Calculations of an α-β pair require lengthy summations, (8), that involve 80 terms (48 O_2 + 30 H_2O lines + 1 dry air + 1 water vapor continuum). By limiting the highest frequency to 300 GHz and considering only local lines that, in addition, display a sufficient absorption strength, the computational effort can be reduced to 40 terms. The modified code is labeled MPM* and operates with the line base LB* (see Table 1) encompassing 34 O_2 + 3 H_2O lines.

Errors of MPM* predictions with reference to MPM were assessed by fitting a data matrix $\Delta\alpha(f, p, T, \text{RH}) = \alpha(\text{LB}) - \alpha(\text{LB*}) = \Delta\alpha_d + \Delta\alpha_v$, that was evaluated for $f = 25$–300(25), $p = 20$–100(20)($h < 12$ km), $T = 260$–300 (20), and RH = 0–100 (25), where the digits in parentheses indicate the step size of the parameterization. The dry air result was $\Delta\alpha_d \cong 0$ with less than 1% error and confined to the 50–70 GHz range. The water vapor error term $\Delta\alpha_v = 0.182 f \Delta N_e''$ is substantial, as shown for an example in Figure 4. An absorption correction

$$\Delta N_e'' \cong 2.9 p e^{1.1} \theta^2 f^{1.5} 10^{-8} \tag{25}$$

was formulated to fit approximately the $\Delta\alpha_v$ data. Prediction errors with MPM* stay below 5% when (25) is added to the water vapor continuum (14*a*).

The second water vapor continuum (25) clearly demonstrates that H_2O lines outside a frequency range of interest cannot be neglected, thus adding support to an interpretation of (14*a*) as being largely a far-wing contribution from the complete water

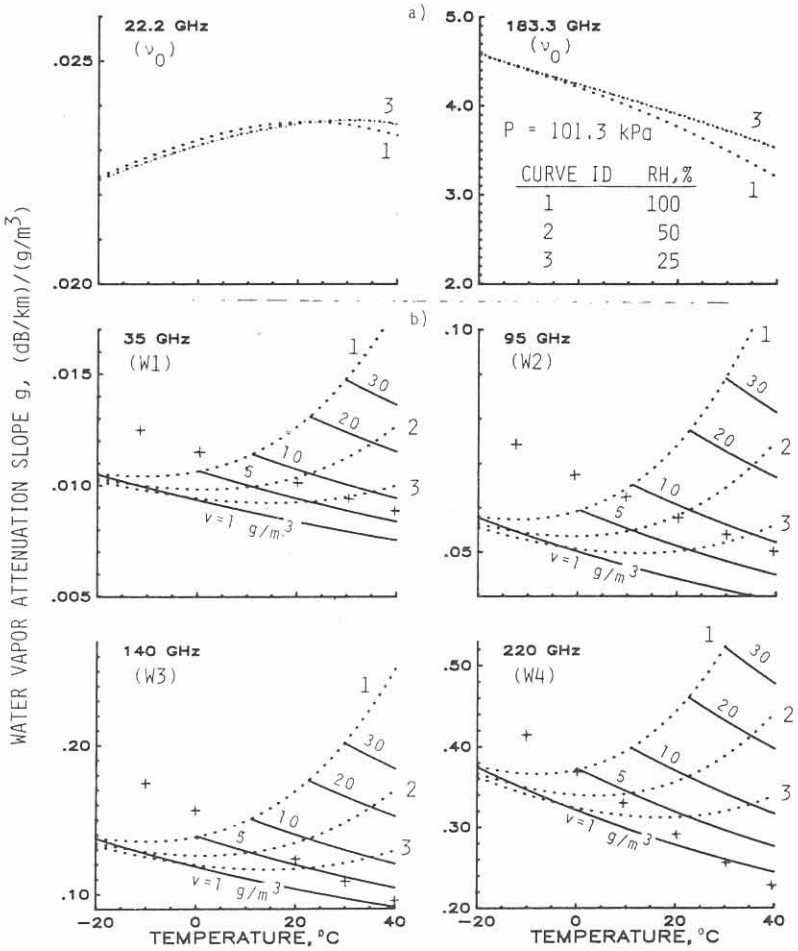

Fig. 3. Water vapor attenuation slope $g(T)$ as a function of temperature (solid curves are v = const, dashed curves are RH = const) at different frequencies: (*a*) H_2O line center frequencies; (*b*) atmospheric transmission windows; + Gaut-Reifenstein continuum.

vapor spectrum. Individual absorption peaks α_0 of H_2O lines above 1 THz reach very high values ($< 10^6$ dB/km), so that residuals of (10^{-6} to 10^{-8})α_0 make measurable contributions in the millimeter wave range. The correct theoretical prediction of these residuals is an area of active research (see section 3.4). A problem of this nature does not exist for the O_2 spectrum since the line peaks do not exceed 50 dB/km for $p \leq 100$ kPa.

The MPM can serve as a reference to even more drastic reductions in computer effort when specific applications are limited to narrow frequency ranges. Atmospheric transparency in the millimeter wave window ranges (W1 to W4), for example, can be evaluated with simple two- or three-coefficient models of α_d (dry air) and α_v [*Liebe*, 1983*b*]. Attenuation behavior in the core region of local lines ($\nu_0 \pm \gamma$) can be approximated by the isolated line contribution. At the center ($f = \nu_0$) of water vapor lines, attenuation peaks with (5), (8*a*), (9*a*), (10), (11), and Table 1 to a value

$$\alpha_0 = 0.182 \nu_0 S/\gamma = k_0 \theta^y e/(4.80e + p) \quad \text{dB/km} \quad (26)$$

where $k_0 = 0.182 \nu_0 b_1/b_3$ and $\theta^{2.5} \exp [b_2(1 - \theta)] \cong \theta^y$. Results for three examples are

$\nu_0 =$ 22.2	183.3	488.5	GHz
$k_0 =$ 15.7	2567	852	dB/km
$y \cong$ 0.25	2.1	−0.3	

Each line contribution has an individual behavior with respect to temperature (and pressure) variations.

TABLE 3. Predicted Specific Attenuation α (dB/km) for a Total Pressure $P = 101.3$ kPa and Hydrosol Attenuation Factor x_w at Various Relative Humidities RH (%) and Temperatures T (K) for Selected Millimeter-Wave Frequencies

Parameters			Hydrosol Factor	Specific Attenuation α of Air, dB/km				
f, GHz	T, K	v_s, g/m^3	x_w (24)	100% RH	75% RH	50% RH	25% RH	0% RH
22.2 (v_0)	310	43.46	8.4	1.03	0.78	0.52	0.27	0.011
	300	25.49	10	0.62	0.46	0.31	0.16	0.012
	290	14.31	13	0.35	0.27	0.18	0.10	0.013
	280	7.65	17	0.19	0.15	0.10	0.06	0.014
	270	3.87	22	0.11	0.08	0.06	0.04	0.016
	260	1.85	29	0.06	0.05	0.04	0.03	0.017
35.0 (W1)	310	43.46	26	0.76	0.50	0.29	0.13	0.026
	300	25.49	41	0.38	0.27	0.17	0.09	0.028
	290	14.31	60	0.20	0.15	0.10	0.06	0.031
	280	7.65	84	0.12	0.09	0.07	0.05	0.034
	270	3.87	114	0.08	0.07	0.06	0.05	0.038
	260	1.85	135	0.06	0.06	0.05	0.05	0.042
95.0 (W2)	310	43.46	28	4.56	2.89	1.58	0.63	0.036
	300	25.49	44	2.18	1.44	0.83	0.37	0.040
	290	14.31	62	1.05	0.73	0.45	0.22	0.044
	280	7.65	79	0.53	0.38	0.26	0.14	0.048
	270	3.87	90	0.28	0.21	0.16	0.10	0.053
	260	1.85	89	0.16	0.14	0.11	0.08	0.058
140.0 (W3)	310	43.46	24	10.21	6.48	3.54	1.39	0.019
	300	25.49	35	4.88	3.21	1.84	0.78	0.021
	290	14.31	46	2.34	1.60	0.97	0.44	0.023
	280	7.65	53	1.13	0.80	0.51	0.25	0.025
	270	3.87	54	0.56	0.41	0.27	0.15	0.027
	260	1.85	48	0.28	0.21	0.15	0.09	0.029
183.3 (v_0)	310	43.46	3.0	143.08	109.98	75.43	38.96	0.014
	300	25.49	2.9	91.32	69.60	47.22	24.07	0.016
	290	14.31	2.7	54.94	41.59	28.01	14.16	0.017
	280	7.65	2.5	31.10	23.44	15.71	7.91	0.018
	270	3.87	2.1	16.54	12.44	8.32	4.18	0.019
	260	1.85	1.7	8.24	6.19	4.14	2.08	0.020
220.0 (W4)	310	43.46	18	26.23	16.73	9.19	3.62	0.016
	300	25.49	23	12.64	8.35	4.81	2.04	0.018
	290	14.31	27	6.10	4.18	2.52	1.14	0.019
	280	7.65	28	2.97	2.10	1.32	0.63	0.021
	270	3.87	25	1.45	1.06	0.69	0.34	0.022
	260	1.85	20	0.70	0.53	0.35	0.19	0.023
Curve ID (Figure 2, Figure 3)			9 ...	8 1	7 ...	6 2	5 3	1 ...

3.3. *MPM predictions versus experimental data*

Corroborative experimental data of sufficient quality to test seriously predictions are scarce. Imperfections in the experimental apparatus, as well as reliability, precision, and limited scope of supporting meteorological data often compromise the accuracy of results deduced from field observations. Generally, laboratory experiments provide more precise tests by simulating controlled electromagnetic and atmospheric conditions crucial to model validations. In this manner, contributions from the 22 and 183 GHz H_2O and 48–70, 119 GHz O_2 lines have been evaluated as summarized by *Liebe* [1981, 1983*a*]. Confirmation is lacking in window ranges W2 to W5 (see Figure 2) that are sensitive to the water vapor con-

TABLE 4. Zenith Attenuation $A_z(f)$ and Delay $B_z = B_0 + B(f)$ Predicted for a Model Summer Atmosphere (30°N, July)

		Attenuation $A_z(f)$, dB				Dispersive Delay $B_z(f)$, ps			
	Frequency, GHz	RH = 0%, V = 0 cm*,†	RH = 50%, V = 3.512 cm†	RH = 75%, V = 5.269 cm†	RH = 100, V = 7.025 cm†	RH = 0%, V = 0 cm, B_0 = 7645 ps	RH = 50%, V = 3.512 cm, B_0 = 8349 ps	RH = 75%, V = 5.269 cm, B_0 = 8701 ps	RH = 100%, V = 7.025 cm, B_0 = 9053 ps
W1	30	0.09 (5.40)	0.40 (2.38)	0.59 (2.20)	0.80 (2.09)	0.27	0.20	0.17	0.14
	40	0.24 (5.36)	0.58 (2.65)	0.81 (2.34)	1.08 (2.15)	2.17	2.41	2.53	2.64
	50	1.34 (5.09)	1.82 (3.57)	2.16 (3.09)	2.57 (2.75)	8.78	9.29	9.54	9.80
	55	27.45 (7.04)	27.86 (6.75)	28.18 (6.52)	28.59 (6.26)	26.20	26.80	27.10	27.40
O_2	60	149.30 (11.08)	149.10 (11.03)	149.20 (10.93)	149.30 (10.80)	0.63	1.56	2.02	2.48
	65	22.61 (6.21)	23.29 (5.83)	23.80 (5.55)	24.41 (5.25)	−32.10	−30.80	−30.10	−29.50
	70	1.62 (4.96)	2.55 (3.17)	3.20 (2.74)	3.98 (2.46)	−16.20	−14.80	−14.10	−13.40
	80	0.39 (5.00)	1.57 (2.29)	2.41 (2.08)	3.41 (1.97)	−9.93	−8.08	−7.15	−6.23
W2	90	0.20 (4.96)	1.69 (2.09)	2.75 (1.96)	4.02 (1.89)	−7.97	−5.58	−4.39	−3.20
	100	0.17 (5.08)	2.01 (2.05)	3.32 (1.94)	4.89 (1.87)	−6.98	−3.97	−2.46	−0.96
	110	0.35 (5.62)	2.59 (2.13)	4.18 (1.98)	6.08 (1.90)	−6.20	−2.49	−0.64	1.22
	115	1.39 (6.32)	3.84 (2.59)	5.59 (2.27)	7.67 (2.10)	−5.47	−1.38	0.67	2.72
O_2	120	7.50 (9.42)	10.18 (4.67)	12.08 (3.73)	14.35 (3.15)	−8.57	−4.06	−1.80	0.46
	125	0.50 (5.90)	3.45 (2.15)	5.53 (2.00)	8.02 (1.91)	−6.77	−1.83	0.64	3.11
W3	150	0.05 (4.99)	4.71 (1.98)	7.93 (1.91)	11.70 (1.86)	−5.87	1.76	5.58	9.39
	175	0.04 (5.08)	17.39 (2.17)	27.60 (2.12)	38.70 (2.08)	−5.59	8.01	14.80	21.60
H_2O	185	0.05 (5.18)	120.10 (3.02)	180.20 (3.03)	240.30 (3.03)	−5.52	−3.56	−2.29	−0.84
	200	0.05 (5.35)	11.50 (2.04)	19.00 (1.98)	27.50 (1.93)	−5.43	4.45	9.39	14.30
	225	0.06 (5.60)	10.50 (1.97)	17.70 (1.91)	26.30 (1.86)	−5.33	9.77	17.30	24.90
W4	250	0.07 (5.78)	12.70 (1.97)	21.50 (1.90)	31.90 (1.85)	−5.27	14.70	24.80	34.80
	275	0.09 (5.91)	15.80 (1.98)	26.70 (1.91)	39.60 (1.86)	−5.22	20.40	33.30	46.10
	300	0.11 (6.00)	20.80 (1.99)	34.80 (1.93)	51.20 (1.88)	−5.18	27.50	43.90	60.20
H_2O	325	0.13 (6.06)	237.70 (3.33)	335.00 (3.32)	472.00 (3.30)	−5.14	35.40	55.70	75.90
W5	350	0.17 (6.06)	38.90 (2.05)	63.60 (1.99)	91.80 (1.94)	−5.10	45.00	70.00	95.00

RH, relative humidity (h = 0–8 km); V, integrated water vapor (21); B_0, refractive path delay (19*b*).

*A_0.

†Values in parentheses represent effective height $h_E = A_z/\alpha(h_0)$ km, 42 height levels, h_0 = 0 km (p_0 = 101.35 kPa, T_0 = 301.15 K), and h_f = 30 km.

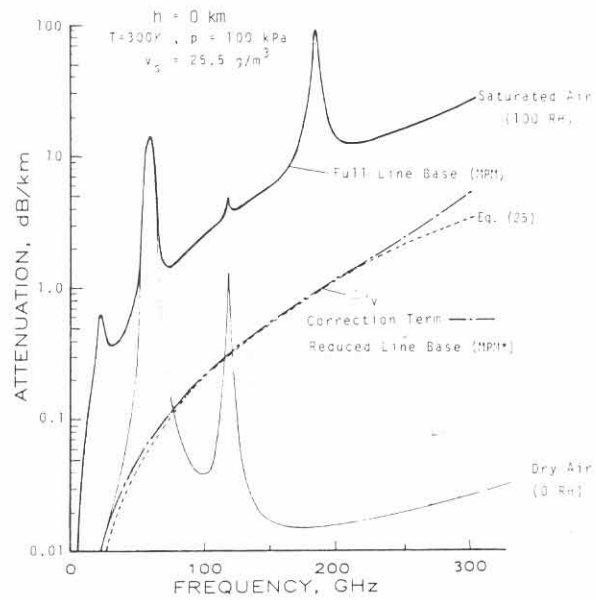

Fig. 4. Example of dry and saturated air attenuation $\alpha(f)$ for simulated sea level conditions and frequencies up to 300 GHz, and the correction term $\Delta\alpha_v$ to be added when using the reduced line data base MPM*.

tinuum (14). To test the MPM program, several suitable data sets on humidity-dependent propagation effects were chosen. The data have been gathered recently under diverse conditions. An overview of the experiments is given in Table 5. Reported data are generally available in graphic form and had to be digitized by us for a comparison with model predictions. Analysis of raw data $\alpha(v, T)$ available from the experiments allows an estimate of their negative temperature dependence θ^y. The exponent y was found to vary between 3.5 and 6, which is consistent with theoretical results (33) to be discussed in the next section.

Dry air attenuation α_d below 40 GHz (see Figure 2) does not exceed the detection threshold of a laboratory spectrometer (typically ≥ 0.05 dB/km). In this range, MPM validations have to rely on field experiments employing long path lengths. Results on zenith attenuation $A_z = A_0 + a_v V + \cdots$ (dB) from 2.5 to 32 GHz fall in this category. Experimental attenuation A_z was deduced from radiometric measurements of atmospheric brightness T_B. Two series of radiometer experiments have been evaluated

TABLE 5. Overview of Experimental Efforts Used to Provide Corroborative Data for the Propagation Program MPM

Test Frequency f, GHz	Figure	Path Type	Path Length L, km	Negative Temperature Exponent y	Reference
2.5–90.0	(Table 6)	ZEN	···	···	*a*
20.6	5 (Table 6)	ZEN	···	···	*b*
31.6	5 (Table 6)	ZEN	···	···	*c*
31.8	[*Liebe*, 1983*a*]	LAB	···	···	*d*
81.84	7	LOS	0.81	···	*e*
28.8/96.1	6	LOS	27.2	5(2)	*f*
110.0	[*Liebe*, 1983*a*]	LAB	···	5.5(8)	*g*
138.2	(equation (34))	LAB	(equivalent 0.15)	4.0(1.5)	*h*
192–260	8	LOS	1.5	3.6(1.3)	*i*
245.52	7	LOS	0.81	···	*e*
337	[*Liebe*, 1983*a*]	LOS	0.50	5(2)	*j*
335–418	9	LOS	1.58	···	*k*
330–430	9	LAB	···	···	*k*

LOS, horizontal line-of-sight path; ZEN, zenith path, LAB, laboratory experiment.
[a]*Costales* [1984]; L. Danese (personal communication, 1984).
[b]D. C. Hogg et al., (personal communication, 1983).
[c]*Hogg et al.* [1983].
[d]*Becker and Autler* [1946].
[e]*Manabe et al.* [1984].
[f]*Liebe et al.* [1985].
[g]*Llewellyn-Jones and Knight* [1981]; *Knight and Llewellyn-Jones* [1982].
[h]*Liebe* [1984].
[i]*Fedoseev and Koukin* [1984].
[j]*Gasiewski* [1983].
[k]*Furashov et al.* [1984].

TABLE 6. Predicted Zenith Attenuation $A_z = A_0 + a_v V$ (18) and Atmospheric Brightness $T_B = T_0 + z_v V$ (20) for Two Series of Radiometer Experiments

Radiometer Experiments			Dry Air Attenuation, dB		Water Vapor Slope, dB/cm			
Center Frequency f_c, GHz	Initial Height h_0, km	Atmospheric Brightness T_B^x, K	A_0	A_0^x	a_v	a_v^x	Total Water Vapor V (21), cm	
20.6	0	···	0.061	0.06(1)*	0.171[1]†	0.190(7)*	0–2.9	0.5–3.2
31.6	0	···	0.121	0.118(6)	0.086[4]	0.089(4)		
20.6	0.9	···	0.051	0.05(1)	0.173[1]	0.188(5)	0–1.9	0.6–3.6
31.6	0.9	···	0.102	0.103(4)	0.077[3]	0.076(2)		
20.6	1.5	···	0.045	0.05(2)	0.175[1]	0.173(2)	0–1.4	0.7–2.5
31.6	1.5	···	0.090	0.093(4)	0.072[3]	0.066(4)		
2.5	3.80	0.95(5)*	0.0157	0.938‡	···	···	···	···
4.75	3.80	1.10(10)	0.0161	0.962‡	···	···	···	···
9.40	3.80	1.03(3)	0.0173	1.034‡	0.0039	0.27§	0.33	0.2–0.4
10.0	3.80	1.15(10)	0.0175	1.046‡	0.0046	0.32§	0.33	0.2–0.4
33.0	3.80	4.51(18)	0.0565	3.361‡	0.0518	3.62§	0.33	0.2–0.4
90.0	3.80	11.00(20)	0.909	5.385‡	0.249	17.0§	0.33	0.2–0.4

Series one: 20.6/31.6 GHz, three initial heights h_0, U.S. Standard Atmosphere, MPM results averaged over $f_c \pm 0.2$ (for details see Figure 5, for references see Table 5); series two: 2.5–90 GHz, one initial height h_0, California Atmosphere, MPM results at f_c (for details see text, for references see Table 5).

*Digits in parentheses give the data uncertainty as standard deviation from the mean.

†Digits in brackets give data variability due to changes in V, both in terms of final listed digits.

‡T_0, K.

§z_v, K/cm.

in some detail as summarized in Table 6. The first was performed at three locations in the United States, where climatic conditions at ground level h_0 varied as follows:

Location	h_0, km		$P(h_0)$, kPa		$T(h_0)$, °C		RH(h_0), %	Data Scatter (rms), dB	
Sterling, Va.	0	0	101.0(5)	101.3	11(6)	15	87(12)	0.030	0.016
N. Platte, Neb.	0.8	0.9	91.8(6)	91.0	19(11)	9	56(25)	0.032	0.017
Denver, Colo.	1.6	1.5	83.8(3)	84.6	21(5)	5	37(16)	0.014	0.008
	exp	MPM	exp	MPM	exp	MPM	exp	20.6	31.6 GHz

The authors [*Hogg et al.*, 1983] fitted straight lines to A_z versus V and obtained A_0^x as intercept at $V = 0$. Any nonlinear behavior of the rate a_v is buried within the data scatter. We could improve somewhat the fit to both values, A_0^x and a_v^x, by enforcing the constraint A_0^x (experiment) $\cong A_0$ (MPM), and those results are given in Table 6. The MPM simulation employed the U.S. Standard Atmosphere (1976), and four water vapor profiles RH(h) to generate V. Graphic results illustrate in Figure 5 the height dependence for dry air attenuation A_0 and water vapor slope a_v. Although no claim can be made that the model atmosphere presents the actual field conditions, a numerical comparison of MPM versus experiment (Table 6) produces, within experimental uncertainty, a satisfactory agreement; only two values of a_v (20.6 GHz, $h_0 = 0$ and 0.8 km) are systematically higher by about 10%. At 20.6 GHz, the 22 GHz H_2O line contributes about 85% to a_v and observed discrepancies are tied to the line response. Three explanations can be offered for enhanced a_v values: (1) meteorological data are vastly different from modeling assumptions, (2) center frequency of the radiometer is slightly (0.1–0.2 GHz) higher, or (3) line strength ($b_1 = 0.109$) and width ($b_3 = 27.84$) coefficients (Table 1) are in error. Water vapor results at 31.6 GHz are dominated (about 70%) by the nonlinear continuum (14*a*).

The second series of radiometer experiments were conducted from a mountain peak (White Mountain,

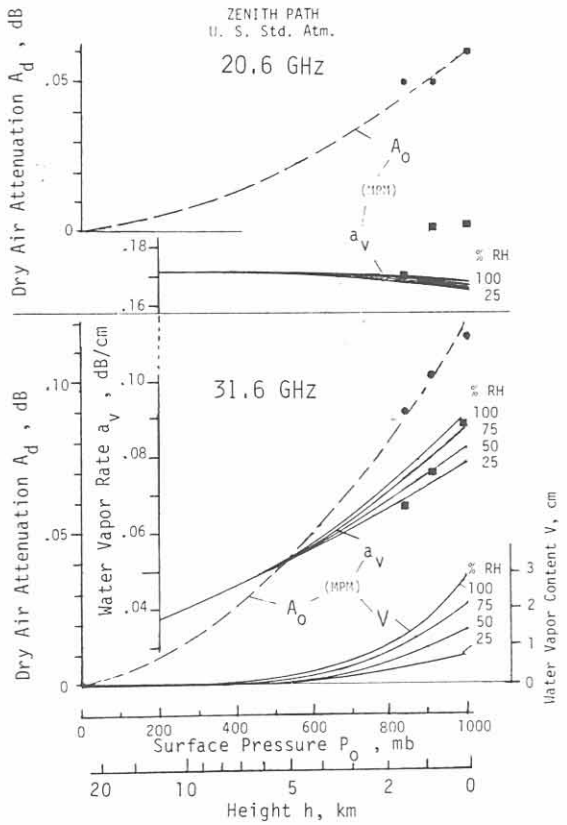

Fig. 5. Dry air attenuation A_0 and water vapor attenuation slope a_v at 20.6 and 31.6 GHz, predicted for a zenith path through the U.S. Standard Atmosphere assuming four water vapor contents $V(h)$ and displayed as a function of height h or surface pressure P_0. Also shown are dry air (circles) and water vapor slope (squares) attenuation values measured from three height levels h_0 at 20.6 and 31.6 GHz (see Table 6).

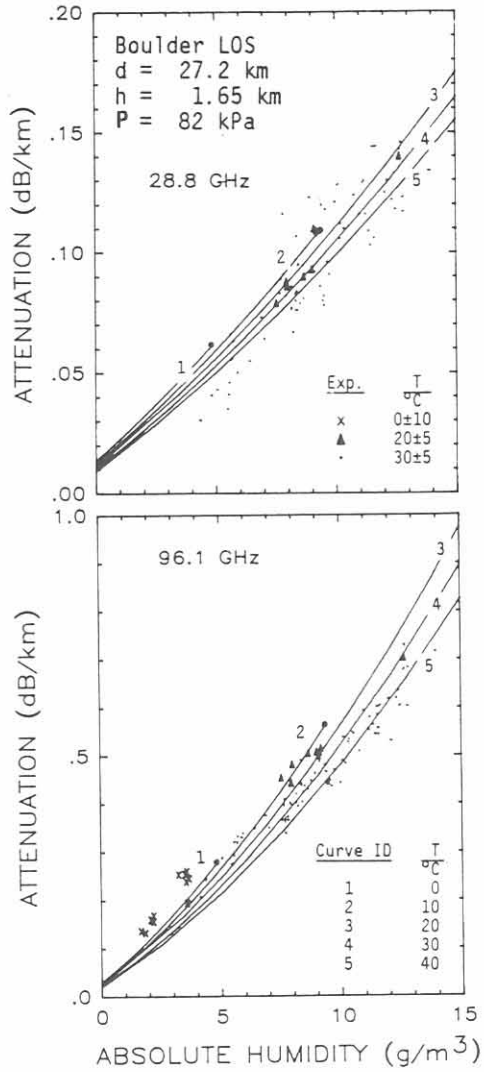

Fig. 6. Specific attenuation at 28.8 and 96.1 GHz at five different temperatures (0° to 40°C): crosses, triangles, dots measured data (14 ± 22°C) [*Liebe et al.*, 1985]; lines MPM; circles, RH = 100%.

California, $h_0 = 3.80$ km, clear weather, $P_0 = 65$ kPa, $T_0 = 6 \pm 5$°C) with utmost care for the purpose of measuring cosmic background radiation (2.7 K). At $h_0 = 3.80$ km, a typical water vapor content is reduced to about $V \cong 0.3 \pm 0.1$ cm. Reported is the atmospheric brightness T_x at 2.5, 4.75, and 9.40 GHz by L. Danese (personal communication, September 1984: "Atmospheric Emission: Models, Comparison With Data, Consequences on Measurements of T_{CBR}," Istituto di Astronomia, Padova, Italy) and at 10, 33, and 90 GHz by *Costales* [1984]. The MPM program was applied to a mean July climate for California specifying $P(h)$, $T(h)$ and $v(h)$ profiles over the range $h = 3.8$–30 km. By numerical integration, dry air zenith attenuation A_0 and a water vapor attenuation slope a_v were calculated as listed in Table 6. Values of A_0 have been converted into brightness temperatures $T_0 = 260(1-10^{-0.1A_0})$, assuming an average medium temperature of 260 K consistent with the $T(h)$ profile for the dry air medium. Brightness data below 10 GHz are particularly sensitive to the correct value of γ_0 in the dry air continuum (13*a*). Above 10 GHz, the water vapor slope a_v amounts to meaningful values. At 90 GHz, the data point $(T_x - T_0)/0.33 = 17.0$ K/cm was used as reference to define an equivalent water vapor medium temperature of 305 K for conversions from attenuation to brightness slope z at other frequencies. This way, all six T_x data in Table 6 are apportioned in consistent

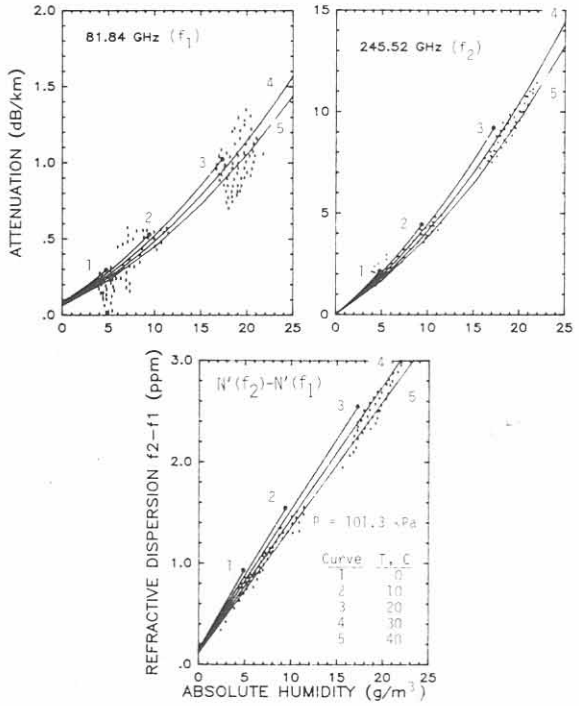

Fig. 7. Specific attenuation α and refractive dispersion $\Delta N = N'(f_2) - N'(f_1)$ for air at temperatures ranging from 0° to 40°C and two frequencies $f_{1,2}$ measured in Tokyo, Japan: rectangles, representative of measured data clusters [*Manabe et al.*, 1984]; lines, MPM; circles, RH = 100%.

manner to dry and wet attenuation terms based upon MPM predictions.

Field data on specific attenuation α are compared with MPM predictions in Figures 6–9. Attenuation data shown in Figure 6 have been measured at 28.8 and 96.1 GHz. The 135 data points represent hourly means from 97 days during stationary conditions, usually afternoons. The data are organized into three temperature groups and compared with MPM predictions. Generally, good agreement is found within the uncertainties (± 0.05 dB/km) of the experiment.

The next example, Figure 7, is unique: attenuation rates $\alpha(v)$ are reported at $f_1 = 81.84$ and $f_2 = 245.52$ GHz together with data on the associated differential dispersion $\Delta N(v) = N'(f_2) - N'(f_1)$. The curves in Figure 7 were produced by inserting reported meteorological conditions into the MPM program and then superimposing the experimental data. Cluster of original points were condensed in dots in the course of the digitizing process. Contrasted with the attenuation rates $\alpha(v)$, an almost linear dependence with absolute humidity v can be observed for dispersion $\Delta N(v)$. The stability of this line-of-sight (LOS) experiment was estimated to be better than ± 0.3 dB/km for α and ± 0.1 ppm for ΔN over a temperature range of 0° to 40°C.

Water vapor attenuation data for frequencies between 195 and 340 GHz are compared with model predictions in Figures 8 and 9. Results for the range $f = 330$–430 GHz include field (8.5°C, 8.4 g/m^3, 99% RH) and laboratory (25.5°C, 19 g/m^3, 80% RH) data taken in the U.S.S.R. (Figure 9). Considering the multifarious difficulties that plague absolute calibrations, the comparisons of model versus experimental data are encouraging. No anomalous absorption features have been uncovered.

In summary, good agreement between predicted and reported responses, foremost specific attenuation, was found over a wide range of parameter choices; test frequencies varied between 2.5 and 430 GHz and meteorological conditions as follows: $P = 70$–101 kPa, $T = -10$–35°C, $v = 0$–40 g/m^3 and $V = 0$–3.5 cm. All in all, some credibility can be given to the computer program MPM detailed in section 2.

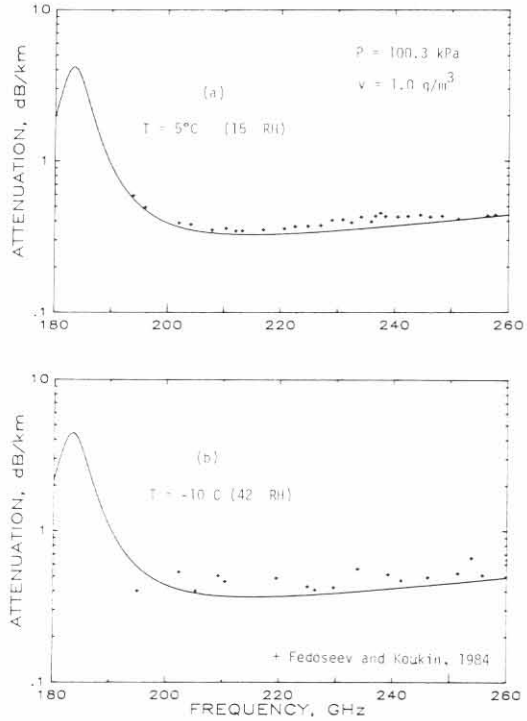

Fig. 8. Water vapor attenuation rates $\alpha(v)$ across the atmospheric window range W4 at two temperatures, 5° and −10°C: pluses, measured data [*Fedoseev and Koukin*, 1984]; lines, MPM.

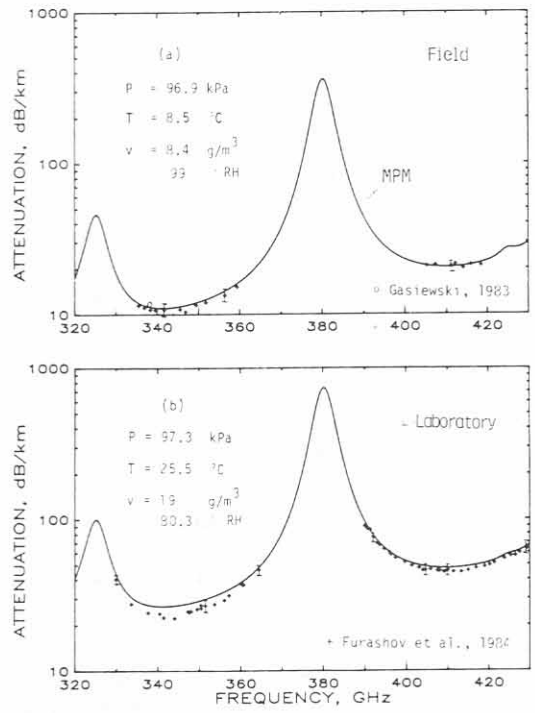

Fig. 9. Water vapor attenuation rates $\alpha(v)$ across the atmospheric window ranges W5 and W6 at two temperatures, 8.5° and 25.5°C: pluses, measured data [*Furashov et al.*, 1984]; open circle, measured [*Gasiewski*, 1983]; lines, MPM.

3.4. *Theoretical H_2O spectrum versus experimental data*

Specific attenuation α_v and refractivity N_v (see (7)) due to the rotational water vapor spectrum can be written in molecular quantities as

$$\alpha_v = 4.343\ M \sum_i (S_M F)_i \qquad \text{dB/km} \tag{27a}$$

and [*Chamberlain*, 1967; *Hill et al.*, 1982]

$$N_v = 22.77 \times 10^6 M' S_B / v_B^2 \qquad \text{ppm} \tag{27b}$$

where the molecular density

$$\begin{aligned} M &= 2.415 e\theta 10^{22} && \text{molec/cm}^2\ \text{km} \\ M' &= M/10^5 && \text{cm}^{-3} \end{aligned} \tag{28}$$

is derived from the ideal gas law, the integrated band strength is $S_B = 5.21 \times 10^{-17}\ \theta$ cm^{-1} $(\text{molec/cm}^2)^{-1}$ [*Rothman et al.*, 1983], and the band center frequency follows to be $v_B = 2624$ GHz.

The line-by-line summation (27*a*) considers each line i that contributes in the frequency range of interest by its strength $S_M(17)$ and shape function

$$F = F''(f)/\pi \qquad \text{cm} \tag{29}$$

Clough et al. [1981] performed calculations of α_v (27) by considering $i \cong 17{,}000$ H_2O lines up to 150 THz from the AFGL tape [*Rothman et al.*, 1983], as opposed to $i = 30$ for the MPM. In addition, the line shape function F (29) included terms to account empirically for a finite duration of molecular collisions [*Clough et al.*, 1983]. Actually, the spectral density function

$$c(f) = \alpha_v(f)/f \tanh x \qquad \text{dB/km GHz} \tag{30}$$

with $x = (f/12510)\theta$ was evaluated, defining the power absorbed per molecule and frequency interval, here given in radio engineering units. Water vapor attenuation $\alpha_v(f)$ can be separated in local line contributions α_l within "small" (25 $\text{cm}^{-1} \equiv 0.75$ THz) intervals and a continuum

$$\begin{aligned} \alpha_c(f) &= \alpha_v - \alpha_l = 4.343 M f(\tanh x) \\ &\cdot [e c_s(f) + p c_f(f)]/P_r \qquad \text{dB/km} \end{aligned} \tag{31}$$

covering the "bottom line" of the complete band spectrum. Although full details of the modified shape F are not given, *Clough et al.* [1981] present graphic results for the spectral density of moist nitrogen up to 90 THz. For a reference pressure $P_r = 101.3$ kPa, the self-broadening (H_2O-H_2O) term $c_s(f)$ and the nitrogen-broadening (H_2O-N_2) term $c_f(f)$ are shown, including a temperature dependence based on 12–70 THz experimental data reported for $T = 296$–358 K by *Burch* [1982]. We read for the frequency range below 1 THz:

$$\begin{aligned} c_s &\cong 1.3\ \theta^{3.5} 10^{-21} \\ c_f &\cong 9.0\ \theta^{0.5} 10^{-23}\ \text{cm}^2/\text{cm}^{-1}\ \text{molec atm} \end{aligned} \tag{32}$$

Inserting (28) and (32) in (31), converting cm^{-1} into GHz, and making use of the approximation $\tanh x \cong x (x \ll 1)$ allows (31) to be expressed as

$$\alpha_c = f^2 (3.6 e^2 \theta^{5.5} + 0.25 e p_1 \theta^{2.5}) 10^{-6} \qquad \text{dB/km} \tag{33}$$

a form amenable to experimental testing.

A well-controlled experiment was conducted at $f_x = 138.2$ GHz, a frequency remote from local lines. Specific attenuation α_v of moist nitrogen was measured for RH = 80–100% and $p_1(N_2) = 0$–120 kPa, yielding [*Liebe*, 1984]

$$\alpha_v^x = 0.197 e^2 \theta^y + 0.0075 e p_1 \theta^{y'} \qquad \text{dB/km} \tag{34}$$

where $y = 5.5 \pm 2$ (based on revised data at 282 K) and $y' = ?$ (not measured). This result is the basis for equation (14*a*). Local line contributions from (5*a*), (8*a*), (9*a*), (10)–(12) at f_x and $\theta = 1$ amount to $\alpha_l =$

$0.0093e^2 + 0.0022ep_1$, leaving the MPM continuum contributions in the amount of

$$\alpha_c^x = \alpha_v^x - \alpha_l = 0.19e^2 + 0.0053ep_1 \quad \text{dB/km} \quad (35)$$

In comparison, theory predicts via (33) that $\alpha_c^{TH} \cong 0.069e^2 + 0.0048ep_1$. Temperature exponent y and nitrogen-broadened ep_1 term (−9%) display fairly good agreement; on the other hand, the MPM self-broadening (e^2) term exceeds theoretical predictions by a factor of 2.8. The long-standing controversy about the molecular origin of excess absorption continues unabated.

Following *Burch* [1982], experimental window data of attenuation rates for moist air reported in 10 references (53 data points) for frequencies between 32 and 1020 GHz (including *Becker and Autler* [1946], *Gasiewski* [1983], *Knight and Lewellyn-Jones* [1982], *Llewellyn-Jones and Knight* [1981], *Waters* [1976], and K. A. Aganbekjan and A. Y. Zrazheviskiy, personal communication, 1982) have been fitted by us to ($\theta = 1$)

$$\alpha_x \cong f^2(11e^2 + 0.035f^{0.5}ep)10^{-6} \quad \text{dB/km} \quad (36)$$

Both self-broadening ($\sim e^2$) and air-broadening ($\sim ep$) terms agree quite well with 138 GHz laboratory data (34). Reducing the number of local lines to three led to additional continuum absorption (25) that was fitted by an $f^{2.5}$ dependence. Apparently, the spectral density function $c(f)$ of the atmospheric water vapor spectrum has to be factored out for contributions from three frequency intervals; that is, from local lines ($\Delta f \cong 10$ GHz), from far wings ($\cong 100$ GHz) and from extreme far wings ($\cong 1000$ GHz). Results formulated by (33) to (36) allow only in part an interpretation of millimeter wave continuum absorption as low frequency far-wing contribution stemming from the pressure broadened H_2O spectrum. There is a challenge for further theoretical work. To support such efforts, parametric laboratory studies (T = 260–320 K, RH = 0–100%, P = 0–120 kPa) at window frequencies (95, 140, and 220 GHz) are underway at ITS.

4. CONCLUSIONS

Performance predictions by analytical means are important for millimeter-wave systems operating through the atmosphere, since effort and risk in realizing new concepts can be reduced to a large extent. Essential to such general model is a simulation of atmospheric transmission and emission effects. A rigorous treatment of this specific problem requires taking into account the spectral properties of all absorbers within the radio path. For moist air, the MPM is a practical alternative up to 1000 GHz (300 GHz for MPM*). The input is provided by routinely measured meteorological variables. Computing time is optimized by addressing only the main absorbers H_2O and O_2 and by restricting line-by-line calculations to "local" features falling within the frequency range of interest. The reduction in number for spectral line terms is considerable, as indicated below.

	Number of Spectral Lines		
Absorber Molecule	AFGL Tape ν_0 = <150 THz	MPM ν_0 = <1 THz	MPM* ν_0 = <300 GHz
O_2	≈2,200	48	34
H_2O	≈17,000	30	3

Analytical, experimental, and theoretical details have been given as they pertain to the formulation and validation of the program MPM. The model is intended to aid performance predictions; in addition, it may serve as a reference for ongoing research, especially with respect to studies of the physical origin of water vapor continuum absorption. Underlying physical principles are easy to grasp, and tests with realistic data tend to confirm, at least up to 430 GHz, the presented MPM routine. To claim general validity, further theoretical work into the role of attractive forces between colliding H_2O molecules is needed in order to find a plausible physical basis for the water vapor absorption continuum.

Acknowledgments. The author wishes to thank K. C. Allen for his contributions toward practicality of the MPM program and G. R. Hand for his programming efforts. The work was supported in part by the U.S. Army Research Office under contract ARO 111-85 and by the U.S. Army Communications Electronics Engineering Installation Agency (USACEEIA) under Project Order CCC-PO-19-83.

REFERENCES

Allen, K. C., H. J. Liebe, and C. M. Rush, Estimates of millimeter wave attenuation for 18 United States cities, *NTIA Rep. 83*-119, Natl. Telecommun. and Inform. Admin., Boulder, Colo., May 1983.

Becker, G. E., and S. H. Autler, Water vapor absorption of electromagnetic radiation in the centimeter wave-length range, *Phys. Rev.*, *70*(5/6), 303–307, 1946.

Belov, S. P., A. F. Krupnov, V. N. Markov, A. A. Mel'nikov, V. A. Skvortsov, and T. Y. Tret'yakov, Study of microwave pressure lineshifts: Dynamic and isotopic dependences, *J. Mol. Spectrosc.*, *101*, 258–270, 1983.

Blake, L. V., Ray height computation for a continuous nonlinear

atmospheric refractive-index profile, *Radio Sci.*, *3*(1), 85–92, 1968.

Bohlander, R. A., R. W. McMillan, and J. J. Gallagher, Atmospheric effects on near-millimeter-wave propagation, *Proc. IEEE*, *73*(1), 49–60, 1985.

Boudouris, G., On the index of refraction of air, the absorption and dispersion of centimeter waves by gases, *J. Res. Natl. Bur. Stand.*, *67D*(6), 631–684, 1963.

Brussaard, G., E. Damosso, and L. Stola, Characterization of the 50–70 GHz band for space communications, *CSELT Rapp. Tech.*, *XI*(5), 313–326, 1983.

Burch, D. E., Continuum absorption by H_2O, *Fin. Rep. AFGL-TR-81-0300*, Ford Aerosp. and Commun. Corp., Aeronutron. Div., Newport Beach, Calif., March 1982.

Chamberlain, J. E., On the calculation of integrated absorption strengths from refraction data, *J. Quant. Spectrosc. Radiat. Transfer*, *7*, 151–168, 1967.

Chang, A. T., and T. T. Wilheit, Remote sensing of atmospheric water vapor, liquid water, and wind speed at the ocean surface by passive microwave techniques from the NIMBUS 5 satellite, *Radio Sci.*, *14*(5), 793–802, 1979.

Chang, H. D., P. H. Hwang, T. T. Wilheit, A. T. Chang, D. H. Staelin, and P. W. Rosenkranz, Monthly distributions of precipitable water from NIMBUS 7: SMMR data, *J. Geophys. Res.*, *89*(D4), 5328–5334, 1984.

Clark, W. W., III, J. E. Miller, and P. H. Richardson, Sky brightness temperature measurements at 135 GHz and 215 GHz, *IEEE Trans. Antennas Propag.*, *AP-32*(9), 928–933, 1984.

Clough, S. A., F. X. Kneizys, L. S. Rothman, and W. O. Gallery, Atmospheric spectral transmittance and radiance: FASCOD1B, *Proc. Soc. Photo Opt. Instrum. Eng.*, *277*, 152–166, 1981.

Clough, S. A., R. W. Davies, and R. H. Tipping, The line shape for collisional broadened molecular transitions: A quantum theory satisfying the fluctuation dissipation theorem, in *Spectral Line Shapes*, vol. 2, pp. 553–568, W. deGruyter, New York, 1983.

Costales, J. B., Simultaneous measurements of atmospheric emission at 10, 33, and 90 GHz, *Rep. LBL-18744*, Lawrence Berkeley Lab., Phys. Div., Berkeley, Calif., November 1984.

Crane, R. K., Fundamental limitations caused by RF propagation, *Proc. IEEE*, *69*(2), 196–209, 1981.

Duncan, L. D., and R. G. Steinhoff, (Ed.), EOSAEL 80 Users Manual, vol. II, *Rep. ASL-TR-0107*, USAERCDC Atmos. Sci. Lab., White Sands Missile Range, N. M., Feb. 1982.

Endo, Y., and M. Mizushima, Microwave resonance lines of $^{16}O_2$ in its electronic ground state, *Jpn. J. Appl. Phys.*, *21*(6), L379–L380, 1982.

Falcone, V. J., Jr., L. W. Abreu, and E. P. Shettle, Atmospheric attenuation in the 30 to 300 GHz region using RADTRAN and MWTRAN, *Proc. Soc. Photo Opt. Instrum. Eng.*, *337*, 62–66, 1982.

Fedoseev, L. I., and L. M. Koukin, Comparison of the results of summer and winter measurements of atmospheric water vapor absorption at wavelengths 1.5 to 1.55 mm, *Int. J. Infrared Millimeter Waves*, *5*(7), 952–964, 1984.

Flaud, J.-M., C. Camy-Peyret, and R. A. Toth, *Water Vapor Line Parameters from Microwave to Medium Infrared*, Pergamon, New York, 1981.

Furashov, N. I., V. Y. Katkov, and V. Y. Ryadov, On the anomalies of submillimeter absorption spectrum of atmospheric water vapor, *Int. J. Infrared Millimeter Waves*, *5*(7), 971–981, 1984.

Gallery, W. O., F. X. Kneizys, and S. A. Clough, Air mass computer program for atmospheric transmittance/radiance calculation, FSCATM, *Rep. AFGL-TR-83-0065*, Air Force Geophys. Lab., Hanscom Air Force Base, Mass., March 1983.

Gasiewski, A. J., Atmospheric propagation loss measurements in the spectral window at 337 gigahertz, *Tech. Rep. MMW 2-83*, Electr. Eng. and Astrophys. Dep., Case Western Univ., Cleveland, Ohio, Aug. 1983.

Haenel, G., The properties of atmospheric aerosol particles as functions of the relative humidity at thermodynamic equilibrium with the surrounding moist air, *Adv. Geophys.*, *19*, 77–188, 1976.

Hill, R. J., R. S. Lawrence, and J. T. Priestley, Theoretical and calculational aspects of the radio refractive index of water vapor, *Radio Sci.*, *17*(5), 1251–1257, 1982.

Hogg, D. C., F. O. Guiraud, and R. E. Westwater, Emission measurements of 21.6 GHz absorption by atmospheric water vapor, *Radio Sci.*, *18*(6), 1295–1300, 1983.

Knight, R. J., and D. T. Llewellyn-Jones, Measurements of water vapour absorption in the RAL untuned cavity, *Res. Note RL-82-051*, Rutherford Appleton Lab., Chilton, Didcot, Oxon, United Kingdom, July 1982.

Lam, K. S., Application of pressure-broadening theory to the calculation of atmospheric oxygen and water vapor microwave absorption, *J. Quant. Spectrosc. Radiat. Transfer*, *17*, 351–383, 1977.

Liebe, H. J., Modeling attenuation and phase of radio waves in air at frequencies below 1000 GHz, *Radio Sci.*, *16*(6), 1183–1199, 1981.

Liebe, H. J., An atmospheric millimeter wave propagation model, *NTIA Rep. 83-137*, Natl. Telecommun. and Inform. Admin., Boulder, Colo., Dec. 1983*a*.

Liebe, H. J., Atmospheric EHF window transparencies near 35, 90, 140, and 220 GHz, *IEEE Trans. Antennas Propag.*, *AP-31*(1), 127–135, 1983*b*.

Liebe, H. J., The atmospheric water vapor continuum below 300 GHz, *Int. J. Infrared Millimeter Waves*, *5*(2), 207–227, 1984.

Liebe, H. J., and T. A. Dillon, Accurate foreign-gas-broadening parameters of the 22-GHz H_2O line from refraction spectroscopy, *J. Chem. Phys.*, *50*(2), 727–732, 1969.

Liebe, H. J., G. G. Gimmestad, and J. D. Hopponen, Atmospheric oxygen microwave spectrum—Experiment versus theory, *IEEE Trans. Antennas Propag.*, *AP-25*(3), 327–355, 1977.

Liebe, H. J., K. C. Allen, G. R. Hand, R. H. Espeland, and E. J. Violette, Millimeter wave propagation in moist air: Model versus path data, *NTIA Rep. 85-171*, Natl. Telecommun. and Inform. Admin., Boulder, Colo., March 1985.

Llewellyn-Jones, D. T., and R. J. Knight, Molecular absorption by atmospheric gases in the 100–1000 GHz region, *IEE Conf. Publ.*, *195*, 81–83, 1981.

Manabe, T., Y. Furuhama, T. Ihara, S. Saito, H. Tanaka, and A. Ono, Measurements of attenuation and refractive dispersion due to atmospheric water vapor at 80 and 240 GHz, *Conf. Dig. 9th Int. Conf. Infrared Millimeter Waves Takarazuka Jpn.*, *F-3-3*, 465–466, 1984.

Messer, J. K., F. C. DeLucia, and P. Helminger, The pure rotational spectrum of water vapor—A millimeter, submillimeter, and far infrared analysis, *Int. J. Infrared Millimeter Waves*, *4*(4), 505–539, 1983.

Messer, J. K., F. C. DeLucia, and P. Helminger, Submillimeter spectroscopy of the major isotopes of water, *J. Mol. Spectrosc.*, *105*(1), 139–155, 1984.

Mingelgrin, U., The microwave dispersion spectrum of O_2, *Mol. Phys.*, *28*(6), 1591–1602, 1974.

Mizushima, M., Absorption of millimeter to submillimeter waves by atmospheric water molecules, *Int. J. Infrared Millimeter Waves*, *3*(3), 379–384, 1982.

Pickett, H. M., E. A. Cohen, and D. E. Brinza, Pressure-broadening of oxygen and its implications for cosmic background measurements, *Astrophys. J.*, *258*, L49–L51, 1981.

Pierluissi, J. H., K. Tomiyama, W. D. Fowler, and R. B. Gomez, Resonant transmittance model for millimeter wave propagation, *IEEE Trans. Antennas Propag. AP-30*(4), 741–746, 1982.

Poynter, R. L., and H. M. Pickett, Submillimeter, millimeter, and microwave spectral line catalogue, *JPL Publ. 80-23*, Jet Propul. Lab., Pasadena, Calif., June 1981.

Rosenkranz, P. W., Shape of the 5 mm oxygen band in the atmosphere, *IEEE Tran. Antennas Propag.*, *AP-23*(4), 498–506, 1975.

Rosenkranz, P. W., Comment on absorption and dispersion in the O_2 microwave spectrum at atmospheric pressures, *J. Chem. Phys.*, *77*(4), 2216–2216, 1982.

Rothman, L. S., R. R. Gamache, A. Barbe, A. Goldman, J. R. Gillis, L. R. Brown, R. A. Toth, J.-M. Floud, and C. Camy-Peyret, AFGL atmospheric absorption line parameters compilation: 1982 edition, *Appl. Opt.*, *22*(12), 2247–2256, 1983.

Setzer, B. J., and H. M. Pickett, Pressure broadening measurements of the 118.750 GHz oxygen transition, *J. Chem. Phys.*, *67*(1), 340–343, 1977.

Simpson, O. A., B. L. Bean, and S. Perkowitz, Far infrared optical constants of liquid water measured with an optically pumped laser, *J. Opt. Soc. Am. Lett.*, *69*(12), 1723–1726, 1979.

Smith, E. W., Absorption and dispersion in the O_2 microwave spectrum at atmospheric pressures, *J. Chem. Phys.*, *74*(12), 6658–6673, 1981.

Smith, E. W., and M. Guiraud, Pressure broadening of the O_2 microwave spectrum, *J. Chem. Phys.*, *71*(11), 4209–4217, 1979.

Smith, E. W., and M. Guiraud, Errata, *J. Chem. Phys.*, *74*(1), 355, 1981.

Smith, E. K., Centimeter and millimeter wave attenuation and brightness temperature due to atmospheric oxygen and water vapor, *Radio Sci.*, *17*(6), 1455–1464, 1982.

Stankevich, K. S., Absorption of sub-millimeter-range radio waves in a dry atmosphere, *Radiophys. Quantum Electron. Engl. Transl.*, *17*, 579–581, 1974.

Steenbeckeliers, G., and J. Bellet, Spectre micro-onde des molécules $H_2O^{16,17,18}$, *C. R. Acad. Sci. Paris*, *273*, B471–B473, 1971.

Stone, N. W., L. A. Read, A. Anderson, I. R. Dagg, and W. Smith, Temperature-dependent collision-induced absorption in nitrogen, *Can. J. Phys.*, *62*, 338–347, 1984.

Thomas, M. E., and R. J. Nordstrom, The N_2-broadened water vapor absorption line shape and infrared continuum absorption, II, Implementation of the line shape, *J. Quant. Spectrosc. Radiat. Transfer*, *28*(2), 103–112, 1982.

Waters, J. R., Absorption and emission by atmospheric gases, in *Methods of Experimental Physics*, vol. 12B, edited by M. L. Meeks, chap. 2.3, Academic, Orlando, Fla., 1976.

Zrazheviskiy, A. Y., Method of calculating atmospheric water vapor absorption of millimeter and submillimeter waves, *Radio Eng. Electron. Phys.*, *21*(5), 31–36, 1976.

H. J. Liebe, National Telecommunications and Information Administration, Institute for Telecommunication Sciences/S3, Boulder, CO 80303.